THE BUCKLEY-LEVERETT EQUATION WITH DYNAMIC CAPILLARY PRESSURE

K. SPAYD* AND M. SHEARER†

Abstract. The Buckley-Leverett equation for two phase flow in a porous medium is modified by including a dependence of capillary pressure on the rate of change of saturation. This model, due to Gray and Hassanizadeh, results in a nonlinear pseudo-parabolic partial differential equation. Phase plane analysis, including a separation function to measure the distance between invariant manifolds, is used to determine when the equation supports traveling waves corresponding to undercompressive shocks. The Riemann problem for the underlying conservation law is solved and the structures of the various solutions are confirmed with numerical simulations of the partial differential equation.

Key words. undercompressive shock, two phase flow, porous medium, conservation law

AMS subject classifications. 35K70, 35L65, 35L67, 76S05

1. Introduction. The Buckley-Leverett equation for two-phase flow in a porous medium was formulated in the 1940s to model the dynamics of water and oil in porous rock or compacted sand [2]. In its original form, the equation is a scalar conservation law expressing the unidirectional nonlinear transport of the two phases through a medium with uniform porosity. Buckley and Leverett effectively use the method of characteristics to solve typical initial value problems and deduce the breakdown of smooth solutions, giving rise to sharp interfaces or shock waves smoothed by the effect of capillary pressure. More recently, versions of the Buckley-Leverett equation have included capillary pressure as a dissipative term [15, 17]. This pressure has typically been treated as though interfacial forces equilibriate on a fast time scale, an assumption brought into question by Gray and Hassanizadeh, who formulated a dynamic capillary pressure law [5, 6].

In this paper, we study solutions of the Buckley-Leverett equation with unidirectional nonlinear transport and dynamic capillary pressure. The equation expresses conservation of mass for the saturation (volume fraction) $u = u(x,t)$ of one of the phases:

$$\frac{\partial u}{\partial t} + \frac{\partial f(u)}{\partial x} = -\frac{\partial}{\partial x}\left[H(u)\frac{\partial}{\partial x}\left(p_e^c(u) - \tau\frac{\partial u}{\partial t}\right)\right]. \tag{1.1}$$

The flux function $f(u)$, known as the *fractional flow rate*, depends on the ratio of relative permeabilities of the two phases, and has a characteristic S-shaped graph (see Figure 2.1a). The dissipation function $H(u)$ (graphed in Figure 2.1b) is positive, but approaches zero at $u = 0, 1$ where one phase is absent. Consequently, the PDE (1.1) is degenerate at $u = 0, 1$. The equilibrium capillary pressure $p_e^c(u)$ is a decreasing function of saturation, and τ is a relaxation time for the dynamic capillary pressure with a linear rate dependence.

There has been much interest recently in refining the Gray–Hassanizadeh dynamic capillary pressure model (see [14] and the references therein), and in exploring properties of wave-like solutions of equation (1.1) [3, 4, 8, 10, 19]. Much of this effort has been expended on characterizing traveling wave solutions under various simplifications and constitutive assumptions. A striking novel feature of the analysis is the presence of traveling waves that are *undercompressive* in the sense of shock waves [7, 11, 13]. In this paper, we analyze traveling wave solutions in the natural case in which relative permeabilities are quadratic functions of saturation. The structure of traveling waves suggests the form of a nonclassical Riemann solver (when capillary pressure is taken to be negligible), in which shock waves are deemed admissible only if they are singular limits of traveling waves.

In §2, we describe the model in more detail, including specific conditions on relative permeabilities. In this section we also characterize traveling waves as heteroclinic orbits of a system of ODEs, and recall conditions

*DEPT. OF MATHEMATICS, N.C. STATE UNIVERSITY, RALEIGH, NC 27695. RESEARCH SUPPORTED BY NSF GRANTS DMS 0604047, DMS 0636590 RTG.

†DEPT. OF MATHEMATICS, N.C. STATE UNIVERSITY, RALEIGH, NC 27695. RESEARCH SUPPORTED BY NSF GRANTS DMS 0604047, DMS 0968258.

for shock and rarefaction waves. In §3, we analyze the planar vector field derived from the traveling wave ODE, using a separation function whose zeroes correspond to undercompressive traveling waves. In §4, we solve the Riemann problem using the information about traveling waves to identify admissible shocks. The solution is not much different from that predicted earlier [7] for a simpler regularization of the conservation law. In §5 we use an implicit finite difference scheme on the PDE (1.1) to demonstrate some of the solutions of the Riemann problem, except that now the solutions are smooth. As expected, the underlying structure of the smooth solutions is predicted by the Riemann solver of §4. A concluding §6 discusses implications of the results of the paper and possible avenues for further investigation. All of the figures and numerical simulations in this paper were generated using MATLAB®.

2. Preliminaries. In this section, we describe the Gray–Hassanizadeh model and outline the derivation of equation (1.1). Traveling wave solutions of the PDE (1.1) correspond to trajectories between equilibria of a system of ODE, presented in §2.2. Finally, in §2.3 we define shock and rarefaction solutions of the scalar conservation law in which the right hand side of (1.1) is set to zero.

2.1. The Gray–Hassanizadeh model. The Gray–Hassanizadeh model of dynamic capillary pressure [5, 6] is based on the observation that capillary pressure should be time dependent. The simplest form of a time-dependent capillary pressure law introduces a linear rate-dependence of capillary pressure p^c on saturation:

$$p^c(u, u_t) = p_e^c(u) - \frac{1}{\Pi^w}\frac{\partial u}{\partial t}. \tag{2.1}$$

In this equation, u is the saturation (volume fraction) of the wetting phase (water), so that for a fully saturated medium, the saturation of the non-wetting phase (oil) is $1 - u$. Capillary pressure at equilibrium is denoted by p_e^c, and Π^w is a positive material constant.

Let p^j denote the pressure in the jth phase ($j = n, w$), with velocity v^j, and mobility λ^j. Then Darcy's law is

$$v^j = -\lambda^j \frac{\partial p^j}{\partial x}. \tag{2.2}$$

The capillary pressure p^c is the difference between the two phase pressures:

$$p^c = p^n - p^w. \tag{2.3}$$

Combining (2.1)–(2.3), we find

$$-\frac{v^n}{\lambda^n} + \frac{v^w}{\lambda^w} = \frac{\partial p_e^c(u)}{\partial x} - \frac{1}{\Pi^w}\frac{\partial^2 u}{\partial x \partial t}.$$

In unidirectional flow, we can now eliminate one of the velocities by defining the total velocity $v^{total} = v^n + v^w$, as in [15]:

$$v^w = \frac{\lambda^w \lambda^n}{\lambda^w + \lambda^n}\left(\frac{\partial p_e^c(u)}{\partial x} - \frac{1}{\Pi^w}\frac{\partial^2 u}{\partial x \partial t}\right) + v^{total}\frac{\lambda^w}{\lambda^w + \lambda^n}. \tag{2.4}$$

In what follows, we assume v^{total} is constant, a parameter setting the velocity scale. The mobilities λ^j depend on the total permeability constant $K > 0$, and on the relative permeabilities $k^n(1-u), k^w(u)$. These are increasing functions of their respective saturations, since the presence of one phase inhibits the flow of the other phase. Specifically,

$$\lambda^n = \frac{K k^n(1-u)}{\mu^n}, \qquad \lambda^w = \frac{K k^w(u)}{\mu^w}, \tag{2.5}$$

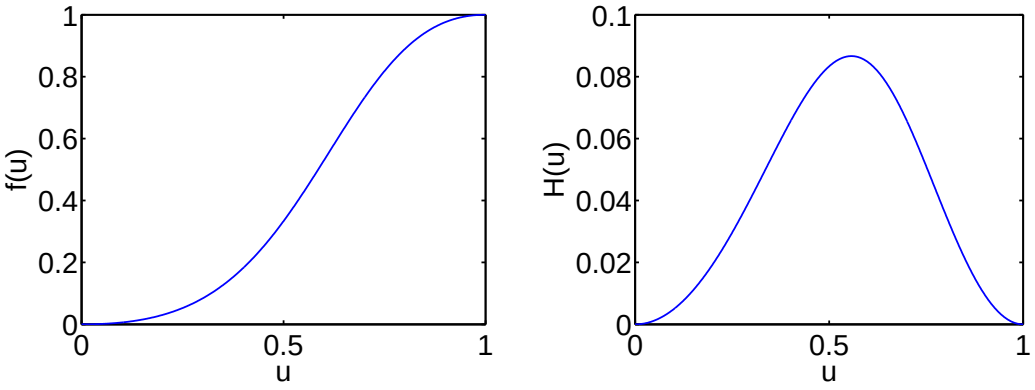

(a) (b)

Fig. 2.1: (a) Fractional flow rate $f(u)$. (b) Capillary induced diffusion $H(u)$ in (2.6)

in which μ^n, μ^w are the viscosities.

Substituting (2.4), (2.5) into the equation for conservation of mass of the wetting phase:

$$\phi \frac{\partial u}{\partial t} + \frac{\partial v^w}{\partial x} = 0,$$

and nondimensionalizing (as in [14]), gives the PDE (1.1):

$$\frac{\partial u}{\partial t} + \frac{\partial f(u)}{\partial x} = -\frac{\partial}{\partial x}\left[H(u)\frac{\partial}{\partial x}\left(p_e^c(u) - \tau\frac{\partial u}{\partial t}\right)\right]. \tag{2.6}$$

Here, the non-dimensional parameter τ depends on the porosity ϕ and a length scale L : $\tau = \dfrac{K}{\Pi^w L^2 \phi \mu^n}$. The flux $f(u)$, the *fractional flow rate,* and $H(u)$, the *capillary induced diffusion* [4] are given by

$$f(u) = \frac{k^w(u)}{k^w(u) + mk^n(1-u)}, \qquad H(u) = \frac{k^w(u)k^n(1-u)}{k^w(u) + mk^n(1-u)},$$

in which $m = \mu^w/\mu^n$. The equilibrium capillary pressure p_e^c has in fact been scaled by a typical pressure $\bar{p} = \frac{v^{total} L \mu^w}{K}$, and is now dimensionless.

In this paper, we assume that relative permeability functions $k^w(u), k^n(1-u)$ are quadratic: $k^j(u) = \kappa^j u^2$, where $\kappa^j > 0$ is constant, $j = w,\ n$. Then we have the functional forms

$$f(u) = \frac{u^2}{u^2 + M(1-u)^2}, \qquad H(u) = \frac{\kappa^n u^2(1-u)^2}{u^2 + M(1-u)^2}, \qquad M = \frac{\kappa^n}{\kappa^w}m.$$

The fractional flow rate $f(u)$ is a convex-concave function with inflection point at $u_I \in (0,1)$. This is significant when describing the hyperbolic wave structure of solutions, as in [13]. Graphs of these functions are shown in Figure 2.1 for $M = 2, \kappa^n = 1$, representative choices [19]. In this case, $u_I = 0.613$. It is commonly assumed that relative permeability functions may be ideally described by quadratic functions [15], but other fractional powers are sometimes fit to relative permeability curves [18].

The (equilibrium) capillary pressure is generally taken to be a smooth and decreasing function of saturation; for simplicity in this paper, we take it to be linear: $p_e^c(u) = -u$. Then (2.6) becomes

$$\frac{\partial u}{\partial t} + \frac{\partial f(u)}{\partial x} = \frac{\partial}{\partial x}\left[H(u)\left(\frac{\partial u}{\partial x} + \tau\frac{\partial^2 u}{\partial x \partial t}\right)\right]. \tag{2.7}$$

Linearizing about a constant $u = u_e$, we obtain a linear PDE for the perturbation $v(x,t)$ of u_e :

$$v_t + f'(u_e)v_x = H(u_e)(v_{xx} + \tau v_{xxt}). \tag{2.8}$$

Solutions of (2.8) of the form $v = e^{\lambda t}\, e^{ikx}$ are specified by the dispersion relation

$$\lambda + ikf'(u_e) = -k^2 H(u_e) - \lambda k^2 \tau H(u_e).$$

Thus,

$$\lambda = -ik\frac{f'(u_e)}{1 + k^2\tau H(u_e)} - \frac{k^2 H(u_e)}{1 + k^2\tau H(u_e)}.$$

Let $c(k) = \dfrac{f'(u_e)}{1 + k^2\tau H(u_e)}$ and $\mu(k) = \dfrac{k^2 H(u_e)}{1 + k^2\tau H(u_e)}$. Then

$$v = e^{ik(x - c(k)t)}\, e^{-\mu(k)t}.$$

Thus the solution has wave speed $c(k)$ bounded above by the characteristic speed $f'(u_e)$ for all k. Moreover, $\mu(k) \to 1/\tau$ as $k \to \infty$, suggesting that τ is akin to a relaxation time.

2.2. Traveling Waves. A traveling wave solution of (2.7) is of the form $u(x,t) = \tilde{u}(\eta)$, $\eta = x - st$. Substituting into (2.7) gives the third order ODE (omitting tildes)

$$-su' + (f(u))' = [H(u)u']' - s\tau\,[H(u)u'']' \tag{2.9}$$

where $' = d/d\eta$. Integrating (2.9) with boundary conditions

$$u(\pm\infty) = u_\pm, \quad u'(\pm\infty) = 0, \quad u''(\pm\infty) = 0,$$

leads to the second order ODE

$$-s(u - u_+) + f(u) - f(u_+) = H(u)u' - s\tau H(u)u'', \tag{2.10}$$

together with the Rankine-Hugoniot condition

$$-s(u_+ - u_-) + f(u_+) - f(u_-) = 0. \tag{2.11}$$

As in [19], it is convenient to write $\hat{u}(\xi) = u(\eta)$ where $\xi = \eta/\sqrt{s\tau}$. Then equation (2.10) becomes (hats omitted)

$$H(u)u'' - \frac{H(u)}{\sqrt{s\tau}}u' - s(u - u_+) + f(u) - f(u_+) = 0, \tag{2.12}$$

where $' = d/d\xi$. We write (2.12) as a first order system of ODEs:

$$u' = v \tag{2.13a}$$

$$v' = \frac{1}{\sqrt{s\tau}}v + \frac{1}{H(u)}\left[s(u - u_-) - f(u) + f(u_-)\right]. \tag{2.13b}$$

Traveling waves correspond to heteroclinic orbits between equilibria $(u_\pm, 0)$, analyzed in detail in §3.

2.3. Shocks and rarefactions. A *shock wave* from u_- to u_+ with speed s is a discontinuous weak solution of the scalar conservation law

$$u_t + f(u)_x = 0 \tag{2.14}$$

which has the form

$$u(x,t) = \begin{cases} u_- & \text{if } x < st \\ u_+ & \text{if } x > st, \end{cases} \tag{2.15}$$

where s is defined by the Rankine-Hugoniot condition (2.11) as the slope of the chord connecting $(u_-, f(u_-))$ and $(u_+, f(u_+))$. (In this paper we consider only constant $u_\pm, s$; more generally, $u_\pm$ would be one-sided limits at a discontinuity $x = \tilde{x}(t)$ with speed $s(t) = \tilde{x}'(t)$.)

A *Lax shock* is a shock wave which satisfies the Lax entropy condition [12]:

$$f'(u_+) \le s \le f'(u_-), \tag{2.16}$$

so that *characteristics* $x(t) = f'(u_\pm)t + x_0$ converge on the shock from each side.

A shock from u_- to u_+ with speed s is *admissible* if there exists a solution $(u,v)(\xi)$ of (2.13) such that $(u,v)(\pm\infty) = (u_\pm, 0)$. Because of the presence of admissible *undercompressive* shocks, in which characteristics converge on the shock only from ahead of the wave, not all admissible shocks are Lax shocks and not all Lax shocks are admissible.

A *rarefaction wave* is a piecewise smooth weak solution of (2.14) which has the form

$$u(x,t) = \begin{cases} u_- & \text{if } x < f'(u_-)t \\ r(\frac{x}{t}) & \text{if } f'(u_-)t \le x \le f'(u_+)t \\ u_+ & \text{if } x > f'(u_+)t \end{cases}$$

where $u = r(\xi)$ is defined by $f'(u) = \xi$. Note that this makes sense if $f'(u)$ is increasing from $f'(u_-)$ to $f'(u_+)$.

3. Equilibria and heteroclinic orbits. In this section we investigate the structure of heteroclinic orbits for system (2.13) using a combination of analysis and simulation. In §3.1, we describe when there are three equilibria and characterize them as saddles, nodes and spirals. We define a separation function in §3.2 which is used to determine pairs (u_-, u_+) for which there is a saddle-saddle connection. The numerical computation of the separation function is detailed in §3.3. In §3.4, we analytically confirm properties suggested by the numerical calculations.

3.1. Equilibria. Equilibria for system (2.13) are points $(u,v) = (u,0)$, where $s(u-u_-) = f(u) - f(u_-)$; these correspond to points of intersection between the graph of f and the line with slope s through $(u_-, f(u_-))$. In particular, for the shock wave (2.15), $(u_\pm, 0)$ are equilibria. When there are three equilibria, we will denote the corresponding values of u as $u_{bot} < u_{mid} < u_{top}$.

The Jacobian of (2.13),

$$J(u,0) = \begin{pmatrix} 0 & 1 \\ \dfrac{s - f'(u)}{H(u)} & \dfrac{1}{\sqrt{s\tau}} \end{pmatrix},$$

has eigenvalues

$$\lambda_\pm = \frac{1}{2}\left\{ \frac{1}{\sqrt{s\tau}} \pm \sqrt{\frac{1}{s\tau} + 4\frac{s - f'(u)}{H(u)}} \right\}. \tag{3.1}$$

Consequently, the outside equilibria, $u = u_{bot}$ and $u = u_{top}$, are saddle points since $f'(u) < s$. The middle equilibrium u_{mid} is an unstable node or spiral since $f'(u_{mid}) > s$.

By a *saddle-saddle connection* from u_- to u_+ we mean a heteroclinic orbit from $(u_-, 0)$ to $(u_+, 0)$ when $(u_\pm, 0)$ are saddle point equilibria. When $u_{bot} = u_- < u_{top} = u_+$, this saddle-saddle connection occurs in the upper half plane. On the other hand, when $u_{bot} = u_+ < u_{top} = u_-$, the connection lies in the lower half plane. Note that homoclinic orbits are possible only for $\tau = \infty$ since the system is conservative only in this limit.

For each $u_- \in [0, 1]$, consider the equation

$$f'(u) = \frac{f(u) - f(u_-)}{u - u_-}, \quad 0 < u < 1. \tag{3.2}$$

LEMMA 3.1. *Suppose $f : [0,1] \to [0,1]$ is continuous and C^4 on $(0,1)$. Suppose further that $f'(0) = f'(1) = 0$, $(u - u_I)f''(u) < 0$ for $u \neq u_I$ and $f'''(u_I) < 0$. Then there is a continuous function $u_\alpha : [0,1] \to [0,1]$ that is C^4 on $(0,1)$ such that for each $u_- \neq u_I$, $u = u_\alpha(u_-)$ is the unique solution of (3.2); moreover, $u_\alpha(u_I) = u_I$, and $u'_\alpha(u_I) = -\frac{1}{2}$.*

Proof. Let

$$g(u_-, y) := f'(y)(y - u_-) - f(y) + f(u_-) \tag{3.3}$$

with $u_-, y \in (0,1)$. Without loss of generality, we assume $u_- < u_I \leq y$. We begin by showing the existence of $u_\alpha(u_-)$. By the Mean Value Theorem, $f'(z) = \dfrac{f(y) - f(u_-)}{y - u_-}$ for some z depending on y with $u_- < z < y$. Letting $y = u_-$, we have $f'(z) < f'(u_I)$ for all z, $u_- < z < u_I$ so that $f'(u_I) > \dfrac{f(u_I) - f(u_-)}{u_I - u_-}$. Thus $g(u_-, u_I) > 0$. On the other hand, if $y = 1$, then $f'(z) > f'(1) = 0$ so that $g(u_-, 1) < 0$. By continuity, there is a value $u_\alpha(u_-) \in (u_I, 1)$ such that $g(u_-, u_\alpha(u_-)) = 0$. Uniqueness follows from the inequality

$$\frac{\partial g}{\partial y} = (y - u_-)f''(y) < 0 \qquad \text{for } y > u_I. \tag{3.4}$$

Repeatedly differentiating (3.3) and evaluating at $u_- = y = u_I$ leads to $u'_\alpha(u_I) = -\dfrac{1}{2}$. Regularity follows from (3.4) and the Implicit Function theorem except at $u_- = u_I$ where the proof involves taking limits. This completes the proof of Lemma 3.1. ∎

The continuous function u_α has range an interval $I_\alpha = \{u_\alpha(u_-) : u_- \in [0,1]\}$. Let $u_\gamma : I_\alpha \to [0,1]$ be the inverse of u_α. Then $u_+ = u_\gamma(u_-)$ gives the intersection of the tangent through $(u_-, f(u_-))$ with the graph of $f(u)$ (where this intersection is in the unit interval):

$$f'(u_-) = \frac{f(u_\gamma(u_-)) - f(u_-)}{u_\gamma(u_-) - u_-}. \tag{3.5}$$

In Figure 3.1b, we show curves A and B defined by $A = \{(u_\alpha(u_+), u_+) : u_+ \in [0,1]\}$, $B = \{(u_-, u_\alpha(u_-)) : u_- \in [0,1]\}$. The regions between these curves represent pairs (u_-, u_+) for which system (2.13) has three equilibria and $u_\pm$ are corresponding saddle points.

Various phase portraits for which (2.13) has two or three equilibria are illustrated in Figure 3.2. The first three portraits in Figure 3.2 show three equilibria; the outside two are saddles while the middle is an unstable node. The trajectories connecting u_{mid} to u_{bot} and u_{mid} to u_{top} in Figure 3.2a correspond to admissible Lax shocks with $u_- = u_{mid}$. However, in Figure 3.2b, there is no trajectory from u_{mid} to

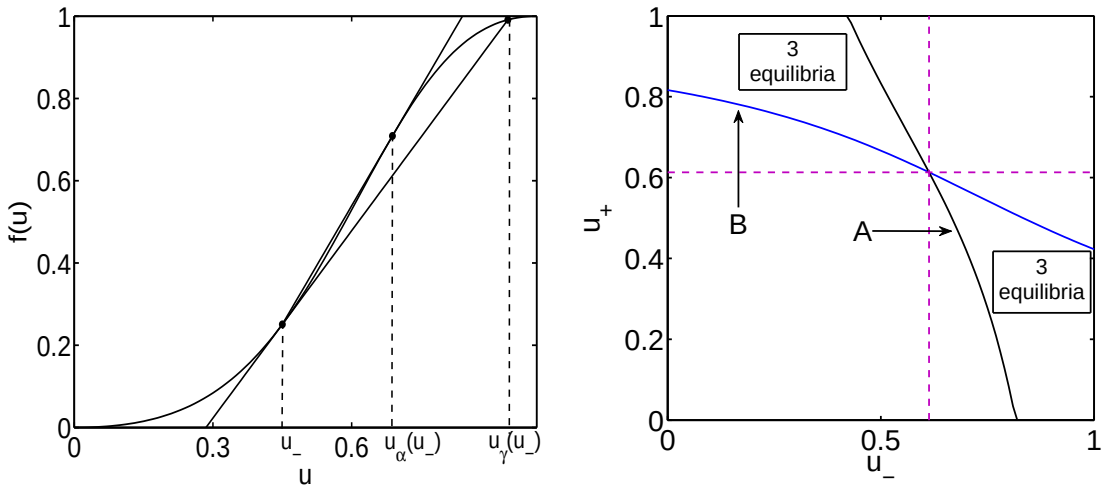

(a) (b)

Fig. 3.1: Values of $u_\pm$ for which there are three equilibria of (2.13); (a) Definitions of $u_\alpha(u_-)$, $u_\gamma(u_-)$ on flux function curve, (b) Graphs A, B of functions $u_\gamma(u_-)$, $u_\alpha(u_-)$, respectively.

u_{top}, even though $u_- = u_{mid}$, $u_+ = u_{top}$ satisfy the Lax entropy condition (2.16). Figure 3.2c illustrates a saddle-saddle connection corresponding to an admissible undercompressive shock between $u_{bot} = u_-$ and $u_{top} = u_+$. This case separates those shown in Figures 3.2a, 3.2b.

Given a pair $(u_-, u_+ = u_\gamma(u_-))$ on curve A, (2.13) has only two equilibria: a degenerate saddle-node at u_- and a saddle at u_+. The two possible phase portraits for such a pair with $u_- < u_I$ are shown in Figures 3.2d, 3.2e. As $u_{bot} = u_-$ and u_{mid} approach each other, Figure 3.2a becomes Figure 3.2d, with the connection between u_{mid} and $u_{top} = u_+$ being preserved, and Figure 3.2b transforms into Figure 3.2e. Between these two cases is a limiting version of Figure 3.2c in which $u_{mid} = u_{bot}$. In contrast to Figure 3.2d there are no trajectories from $(u_{bot}, 0)$ above the stable manifold of $(u_{top}, 0)$.

3.2. Separation function. In this section, we define a separation function $R(\nu)$, for each value of the parameters $\nu = (\beta, s, u_-, M)$ where $\beta = 1/\sqrt{s\tau}$. Zeroes of the separation function determine parameters for which there is a saddle-saddle trajectory from u_- to u_+, where $u_+ \neq u_-$ depends on u_- and s through the Rankine-Hugoniot condition (2.11). The separation function R, defined in [7], measures a distance, at the middle equilibrium, between the unstable manifold emanating from $(u_-, 0)$ and the stable manifold entering $(u_+, 0)$.

Let $\phi = (u, v)$. We use the notation $\nu^0 = (\beta^0, s^0, u_-^0, M^0)$ and $\phi^0 = (u^0, v^0)$ to represent specific values of the parameters and variables. Let $K(\phi; \nu)$ denote the vector field in system (2.13):

$$K(\phi;\nu) = \begin{pmatrix} v \\ \beta v + \frac{1}{H(u)}(s(u-u_-) - f(u) + f(u_-)) \end{pmatrix}.$$

Suppose that for a particular β^0 and pair $u_\pm^0$ (with $u_-^0 < u_+^0$), there is a saddle-saddle connection from u_-^0 to u_+^0 and let $\phi^0(\xi) = (u^0, v^0)(\xi)$ be the corresponding trajectory. That is, $\phi^0(\xi)$ is a solution of (2.13) with boundary values $\phi^0(\pm\infty) = (u_\pm^0, 0)$. For parameter values ν near ν^0, there are saddle points $(u_\pm, 0)$ near $(u_\pm^0, 0)$; the solution of (2.13) along the unstable manifold of the saddle equilibrium at u_- is represented by $\phi_-(\xi; \nu)$ and similarly $\phi_+(\xi; \nu)$ is the solution along the stable manifold of $(u_+, 0)$. We require that $\phi_\pm \in C^1$

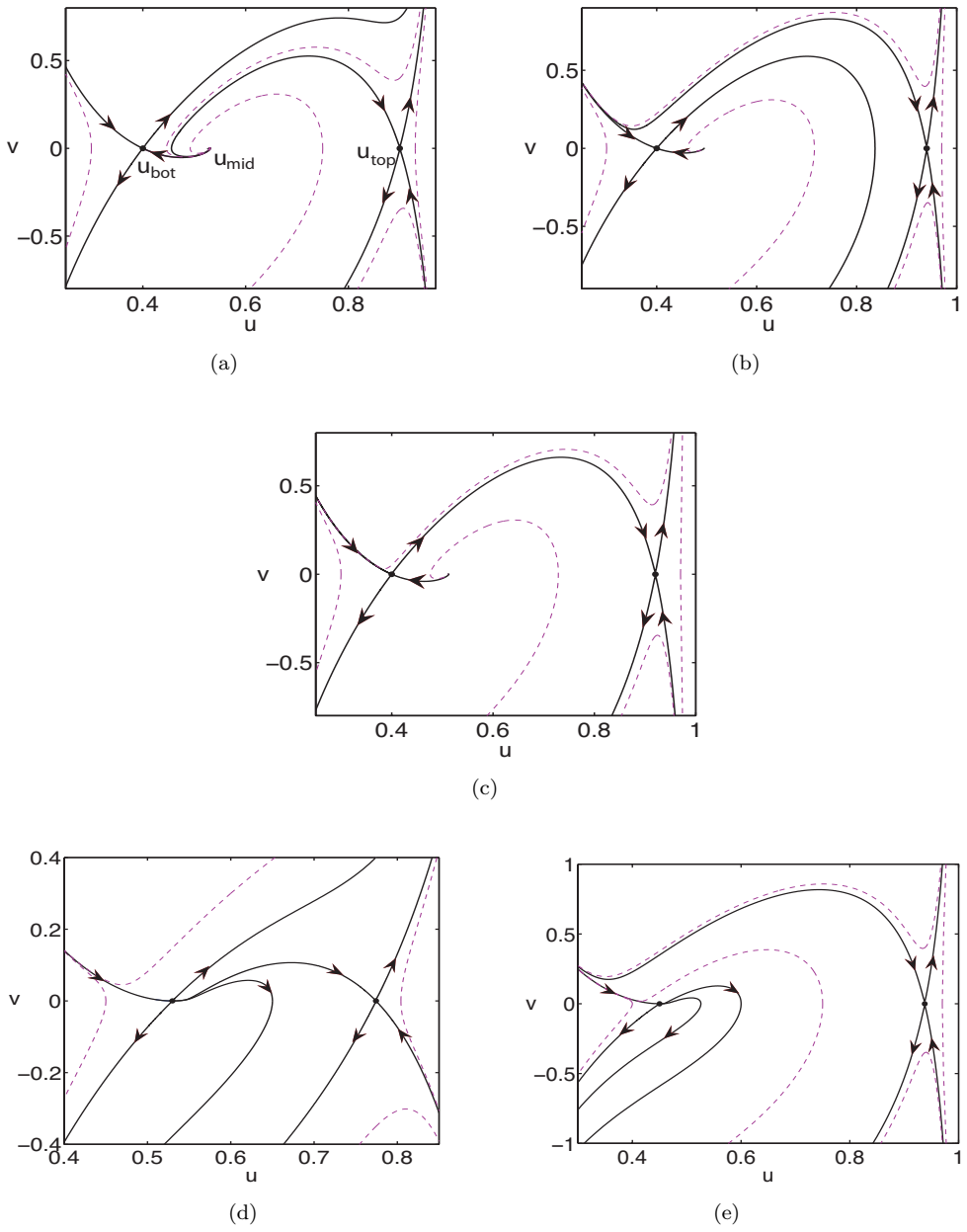

Fig. 3.2: Phase portraits of (2.13) with $M = 2, \tau = 0.1$ for various pairs (u_-, u_+) in the region marked "3 equilibria" in Figure 3.1b, with $u_- < u_I$. (a) The unstable manifold from $u_- = u_{bot}$ is above the stable manifold at $u_+ = u_{top}$. (b) The unstable manifold from u_- is below the stable manifold into u_+. (c) Saddle-saddle connection from u_- to u_+. (d) A single trajectory from the degenerate saddle-node at u_- connects to the saddle at u_+. (e) There is no connection between the degenerate saddle-node at u_- and the saddle at u_+.

in both ξ and ν (near ν^0) and that $\phi_\pm$ satisfy:

$$\phi_-(\xi,\nu^0)=\phi^0(\xi),\ \xi\in(-\infty,0];\quad \phi_+(\xi,\nu^0)=\phi^0(\xi),\ \xi\in[0,\infty)$$
$$\phi_-(-\infty;\nu)=(u_-,0);\qquad \phi_+(\infty;\nu)=(u_+,0).$$

Let $y(\xi)=K(\phi_-(\xi;\nu),\nu)\times\partial_\theta\phi_-(\xi;\nu)$ where $\theta=\beta$, s, u_- or M. (The product $U\times V$ means the 2×2 determinant formed from column vectors U,V.) Then (noting that $\mathrm{div}_\phi K=\beta$) y satisfies the ODE

$$\frac{dy}{d\xi}=\beta y+r(\xi)$$

where $r(\xi)=K(\phi_-(\xi;\nu),\nu)\times\partial_\theta K(\phi_-(\xi;\nu),\nu)$. Solving this linear differential equation by using an integrating factor, we obtain

$$y(0)=\int_{-\infty}^{0}e^{-\beta\xi}r(\xi)d\xi. \tag{3.6}$$

We define the separation function $R(\nu)=K(\phi^0(0),\nu^0)\times(\phi_-(0;\nu)-\phi_+(0;\nu))$; then (3.6) and the corresponding formula for ϕ_+ give

$$\frac{\partial R}{\partial\theta}(\nu^0)=\int_{-\infty}^{\infty}e^{-\beta\xi}\left(K(\phi^0(\xi),\nu^0)\times\frac{\partial K}{\partial\theta}(\phi^0(\xi),\nu^0)\right)d\xi \tag{3.7}$$

for each parameter θ.

Next, we use (3.7) to calculate the sign of each of the derivatives of $R(\nu)$ with respect to the parameters β,u_-,s. First, let $\theta=\beta$. Then we have the following:

$$\frac{\partial K}{\partial\beta}=\begin{pmatrix}0\\ v^0\end{pmatrix},\qquad K\times\frac{\partial K}{\partial\beta}=(v^0)^2.$$

Consequently,

$$\frac{\partial R}{\partial\beta}(\nu^0)=\int_{-\infty}^{\infty}e^{-\beta\xi}(v^0)^2d\xi>0. \tag{3.8}$$

We next consider $\theta=u_-$. Since

$$\frac{\partial K}{\partial u_-}=\begin{pmatrix}0\\ \dfrac{1}{H(u)}(-s^0+f'(u_-^0))\end{pmatrix},\quad K\times\frac{\partial K}{\partial u_-}=\frac{v^0}{H(u^0)}(f'(u_-^0)-s^0),$$

we have:

$$\frac{\partial R}{\partial u_-}(\nu^0)=\int_{-\infty}^{\infty}e^{-\beta\xi}\frac{v^0}{H(u^0)}(f'(u_-^0)-s^0)d\xi<0. \tag{3.9}$$

Finally, for $\theta=s$,

$$\frac{\partial K}{\partial s}=\begin{pmatrix}0\\ \frac{1}{H(u)}(u^0-u_-^0)\end{pmatrix},\qquad K\times\frac{\partial K}{\partial s}=\frac{v^0}{H(u^0)}(u^0-u_-^0).$$

Thus,

$$\frac{\partial R}{\partial s}(\nu^0)=\int_{-\infty}^{\infty}e^{-\beta\xi}\frac{v^0}{H(u^0)}(u^0-u_-^0)d\xi>0. \tag{3.10}$$

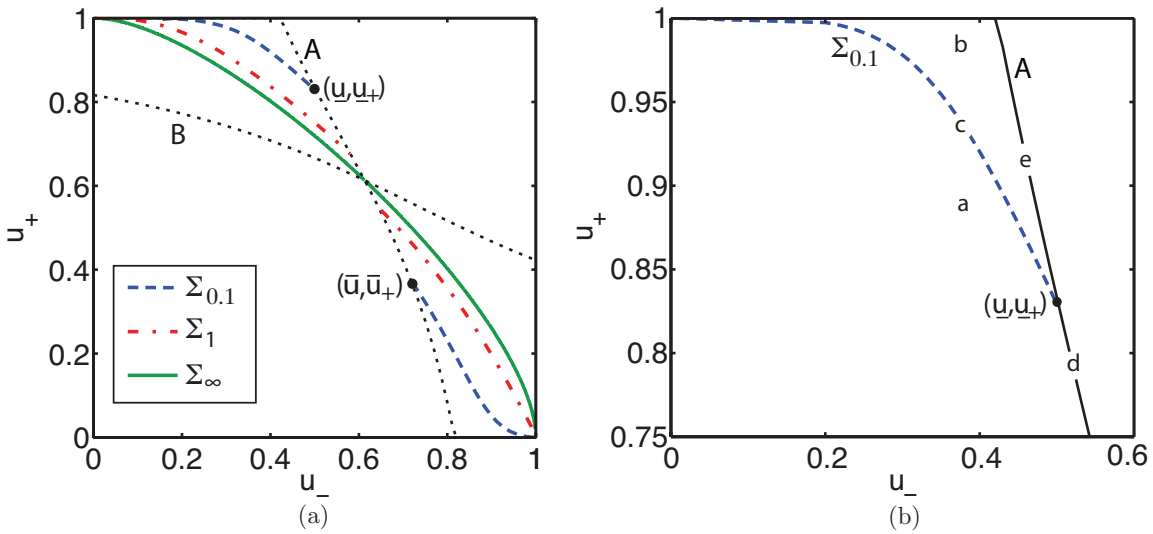

Fig. 3.3: (a) Σ_τ curves for $\tau = 0.1, 1, \infty$. The Σ_τ curves are contained in the region between curves A and B, defined in §3.1. Points $(\bar{u}, \bar{u}_+), (\underline{u}, \underline{u}_+)$ are shown for the case $\tau = 0.1$ only. (b) Region $0 \le u_+ \le u_I \le u_-$ of Figure 3.3a with only curves A and $\Sigma_{0.1}$ shown. The labels a-e refer to corresponding phase portraits in Figure 3.2.

3.3. Numerical calculations. For a fixed $\nu = (\beta, s, u_-, M)$ we compute trajectories $\phi_\pm(\xi;\nu)$ from $\xi = \pm\infty$ respectively, until they cross the vertical line $u = u_{mid}$ at the middle equilibrium. Let $v^m_\pm(\nu)$ denote the corresponding values of v. In practice, we fix τ, M and u_-, and define $\tilde{R}(u_+) = v^m_-(\nu) - v^m_+(\nu)$, in which s varies with u_+. Instead of computing zeroes of $R(\nu)$, we equivalently solve $\tilde{R}(u_+) = 0$.

Our first step is to choose two values of u_+ for which $\tilde{R}(u_+)$ has opposite signs; for $u_- < u_I$, this is the case if we choose $u^{(1)}_+ = u_\alpha(u_-) + \delta$ and $u^{(2)}_+ = u_\gamma(u_-) - \delta$ if $u_- \in I_\alpha$ or $u^{(2)}_+ = 1 - \delta$ if $u_- \notin I_\alpha$, where the small parameter $\delta > 0$ is needed to avoid degenerate equilibria. We then find a zero of $\tilde{R}(u_+)$ by interval division. From (3.10) and the monotonic dependence of s on u_+, we deduce that the zero $u_+ = u_\Sigma(u_-, \tau)$ of $\tilde{R}(u_+)$ is unique (shown in §3.4).

The points $(u_-, u_\Sigma(u_-, \tau))$ lie on a curve Σ_τ, in the u_-, u_+ plane of Figure 3.3; Σ_τ has two connected components that terminate at points $(\underline{u}, \underline{u}_+)$, $(\bar{u}, \bar{u}_+)$ on the curve . In Figure 3.3, we label them only for the case $\tau = 0.1$.

3.4. Properties of the Σ_τ curves. As $\tau > 0$ varies, the Σ_τ curves change as suggested in Figure 3.3. The curves fill a region bounded by the Σ_∞ curve, the curve labeled A and either the u_- axis or the horizontal line $u_+ = 1$. In particular, each Σ_τ curve approaches a corner $(u_-, u_+) = (0, 1)$ or $(u_-, u_+) = (1, 0)$. As observed in [4], for quadratic relative permeabilities there can be no traveling wave connected to an equilibrium with $u_\pm = 0$ or 1. Although there is not a saddle-saddle connection from $u_- = 0$ to $u_+ = 1$, or from $u_- = 1$ to $u_+ = 0$, we can regard the limits of the Σ_τ curves as representing these connections.

We establish the structure seen in Figure 3.3 in two steps: first with $\tau = \infty$ and then $0 < \tau < \infty$. In both cases, we use an identity that involves integrating system (2.13) along a saddle-saddle trajectory from u_- to $u_+ = u_\Sigma(u_-)$ with speed $s = s(u_-, u_+)$ given by the Rankine-Hugoniot condition (2.11). Along a

saddle-saddle trajectory, $v = v(u)$ is a function of u. Then

$$v\frac{dv}{du} = \beta v + \frac{s(u-u_-) - f(u) + f(u_-)}{H(u)}.$$

Let

$$G(u; u_-, s) = \frac{s(u-u_-) - f(u) + f(u_-)}{H(u)}.$$

Then integrating from u_- to $u > u_-$, we have

$$\frac{1}{2}v^2(u) = \beta \int_{u_-}^{u} v(y)\, dy + \int_{u_-}^{u} G(y; u_-, s)\, dy. \tag{3.11}$$

For definiteness, suppose $u_- < u_+$. Then, letting $u = u_+$, and since $v(u) = u' \geq 0$,

$$\int_{u_-}^{u_+} G(y; u_-, s)\, dy = -\beta \int_{u_-}^{u_+} v(y)\, dy \leq 0,$$

with equality only for $\beta = 0$. We define

$$h(u_-, u_+) = \int_{u_-}^{u_+} G(y; u_-, s)\, dy.$$

The equation $h(u_-, u_+) = 0$ gives pairs (u_-, u_+) for which there is a saddle-saddle connection from u_- to u_+ for $\beta = 0$, i.e., in the limit $\tau \to \infty$.

In what follows, it is useful to record the signs of $\dfrac{\partial s}{\partial u_-}$ and $\dfrac{\partial s}{\partial u_+}$ when $u_\pm$ correspond to saddle point equilibria:

LEMMA 3.2. *For $u_- < u_I$ and $u_+ > u_\alpha(u_-)$, $\dfrac{\partial s}{\partial u_+} < 0$ and $\dfrac{\partial s}{\partial u_-} > 0$.*

Proof. We first calculate $\dfrac{\partial s}{\partial u_+}$ from (2.11):

$$\frac{\partial s}{\partial u_+} = \frac{1}{u_+ - u_-}(f'(u_+) - s) < 0,$$

since $u_- < u_+$ and $f'(u_+) < s$. Similarly,

$$\frac{\partial s}{\partial u_-} = \frac{1}{u_+ - u_-}(s - f'(u_-)) > 0.$$

□

PROPOSITION 3.1. *($\tau = \infty$) The level curve $\{(u_-, u_+) : h(u_-, u_+) = 0\}$ is a smooth monotonic curve $u_+ = u_\infty(u_-)$ joining $(u_-, u_+) = (0, 1)$ to $(u_-, u_+) = (1, 0)$. Moreover, $u_\infty(u_-) \sim 1 - u_-^M$ as $u_- \to 0+$ and $u_\infty(u_-) \sim (1 - u_-)^{1/M}$ as $u_- \to 1-$.*

Proof. We begin by establishing the existence of the function $u_+ = u_\infty(u_-)$ such that $h(u_-, u_\infty(u_-)) = 0$. In the following lemma we restrict, without loss of generality, to the interval $0 < u_- < u_I$.

LEMMA 3.3. *For every $u_- < u_I$, there exists a unique $u_+ = u_\infty(u_-) > u_I$ such that $h(u_-, u_+) = 0$. Moreover, $\lim_{u_- \to u_I -} u_\infty(u_-) = u_I$ and $\lim_{u_- \to 0+} u_\infty(u_-) = 1$.*

Proof. We first show that as $u_+ \to 1$ with fixed $u_- < u_I$, $h(u_-, u_+) \to -\infty$. To begin, we observe that

$$G(u; u_-, s) = G(u; u_+, s) = \frac{s(u - u_+) - f(u) + f(u_+)}{H(u)} \tag{3.12}$$

$$= \frac{s(1 - u_+)}{(1-u)^2} - \frac{s}{1-u} + F_1(u, u_+, s) \tag{3.13}$$

where $F_1(u, u_+, s)$ has the property that $\int_{u_-}^{u_+} F_1(u, u_+, s)\, du$ has a finite limit as $u_+ \to 1-$. Consequently,

$$h(u_-, u_+) = \int_{u_-}^{u_+} G(u; u_+, s)\, du \sim s \ln(1 - u_+), \quad \text{as} \quad u_+ \to 1 - . \tag{3.14}$$

On the other hand, for $u_+ = u_I$, the area between the chord joining u_- and u_+ and the curve $f(u)$ is positive (since the chord lies above the graph of f); thus $h(u_-, u_I) > 0$. Since $h(u_-, u_+)$ changes sign, there is a value of u_+ such that $h(u_-, u_+) = 0$. Uniqueness is established by the calculation

$$\frac{\partial h}{\partial u_+} = \int_{u_-}^{u_+} \frac{u - u_-}{H(u)} \frac{\partial s}{\partial u_+}\, du < 0. \tag{3.15}$$

To consider the case near the inflection point, we suppose that u_- is close to u_I. Then $G(u; u_-, s) < 0$ for $u \in (u_-, u_\gamma(u_-))$. Thus $h(u_-, u_\gamma(u_-)) < 0$. Since $h(u_-, u_I) > 0$ (as observed above), we have $u_I < u_\infty(u_-) < u_\gamma(u_-)$. But $u_\gamma(u_-) \to u_I$ as $u_- \to u_I$, so that $\lim_{u_- \to u_I -} u_\infty(u_-) = u_I$.

To show $\lim_{u_- \to 0+} u_\infty(u_-) = 1$, we observe that $h(u_-, u_+)$ for fixed $u_+ < 1$ has the asymptotic form

$$\int_{u_-}^{a} G(u; u_-, s)\, du \sim -sM \ln u_- \quad \text{as} \quad u_- \to 0 + . \tag{3.16}$$

Consequently, since $h(u_-, u_\infty(u_-)) = 0$, we must have $u_+ \to 1$ as $u_- \to 0+$ to avoid the singularity in (3.16). (This idea is pursued more quantitatively below.) This completes the proof of the lemma. □

Next, we show that $u_\infty(u_-) \sim 1 - u_-^M$ as $u_- \to 0+$. We express $h(u_-, u_+)$ with $u_+ = u_\infty(u_-)$ as a sum of three integrals:

$$h(u_-, u_+) = \int_{u_-}^{a} G(u; u_-, s)\, du + \int_{a}^{b} G(u; u_-, s)\, du + \int_{b}^{u_+} G(u; u_-, s)\, du = 0, \tag{3.17}$$

where a and b are chosen such that $\int_a^b G(u; u_-, s)\, du = 0$. Then the first and third terms in (3.17) must balance each other as $u_- \to 0+$ and $u_+ \to 1-$. As in (3.14) and (3.16), respectively,

$$\int_{b}^{u_+} G(u; u_-, s)\, du \sim s \ln(1 - u_+) \quad \text{as} \quad u_+ \to 1- \tag{3.18}$$

$$\int_{u_-}^{a} G(u; u_-, s)\, du \sim -sM \ln u_- \quad \text{as} \quad u_- \to 0 + .$$

The terms from these two integrals must add to zero which gives $u_+ = u_\infty(u_-) \sim 1 - u_-^M$ as $u_- \to 0 + .$

To show monotonicity of $u_\infty(u_-)$, we differentiate the identity $h(u_-, u_\infty(u_-)) = 0$ with respect to u_- and obtain:

$$\frac{\partial h}{\partial u_-} + \frac{\partial h}{\partial u_+} u'_\infty(u_-) = 0.$$

We have that $\dfrac{\partial h}{\partial u_+} < 0$ from (3.15), and we calculate $\dfrac{\partial h}{\partial u_-}$ using (3.12) and Lemma 3.2 with $s = s(u_-, u_+)$:

$$\frac{\partial h}{\partial u_-} = \int_{u_-}^{u_+} \frac{u - u_+}{H(u)} \frac{\partial s}{\partial u_-}\, du < 0.$$

Therefore, $u'_\infty(u_-) < 0$. Defining $u_\infty(0) = 1$ and $u_\infty(u_I) = u_I$, the smooth curve

$$\Sigma_\infty = \{(u_-, u_\infty(u_-)) : 0 \le u_- \le u_I\}$$

decreases monotonically from $(0, 1)$ to (u_I, u_I).

A similar argument for $u_- > u_I$ shows that Σ_∞ extends monotonically from (u_I, u_I) to $(1, 0)$ with $u_\infty(u_-) \sim (1 - u_-)^{1/M}$ as $u_- \to 1-$. This completes the proof of Proposition 3.1. □

In defining the separation function R, it is natural to have it depend on parameters u_-, s, β. However, in the following proposition, we establish properties of the Σ_τ curves in the (u_-, u_+) plane. It is thus convenient to express zeroes of R in terms of parameters $u_\pm, \tau$, so we define

$$\hat{R}(u_-, u_+, \tau) = R(u_-, s(u_-, u_+), \beta), \quad \text{in which} \quad \beta = 1/\sqrt{s(u_-, u_+)\tau}.$$

Note that $\hat{R}$ is not the same as the function $\tilde{R}(u_+)$ used to calculate zeroes of R (see §3.3). The proof of the next proposition uses the inequality

$$\frac{\partial \hat{R}}{\partial u_+}(u_-, u_\Sigma(u_-, \tau), \tau) < 0, \qquad u_- \ne u_I. \tag{3.19}$$

That is, $\hat{R}$ is strictly decreasing in u_+ at the zero $u_+ = u_\Sigma(u_-, \tau)$ of $\hat{R}$. Numerical results show clearly that $\hat{R}(u_-, u_+, \tau)$ is strictly decreasing as a function of u_+, but proving this property is problematic for extreme values of the parameters (specifically large values of τ). Consequently, we make (3.19) an assumption in the proposition.

PROPOSITION 3.2. *($0 < \tau < \infty$) Assuming* (3.19)*, for each $\tau \in (0, \infty)$, there is a $\underline{u} = \underline{u}(\tau)$ with the property that, for each $u_- \in (0, \underline{u})$, the equation $\hat{R}(u_-, u_+, \tau) = 0$ has a unique solution $u_+ = u_\Sigma(u_-, \tau)$. Moreover,*

1. *$u_\Sigma(u_-, \tau)$ is a C^∞ function;*
2. *$\dfrac{\partial u_\Sigma}{\partial \tau} < 0$ and $\dfrac{\partial u_\Sigma}{\partial u_-} < 0$.*

Proof. Let $u_- < u_I$. From Proposition 3.1, let $u_+^0 > u_-^0$ satisfy $h(u_-^0, u_+^0) = 0$. Then $\displaystyle\int_{u_-^0}^{u_+^0} G(y; u_-^0, s^0)\, dy = 0$ and $\displaystyle\int_{u_-^0}^{u} G(y; u_-^0, s^0)\, dy > 0$ for $u_-^0 < u < u_+^0$. The point $(u_+^0, 0)$ is an equilibrium with $s^0 = s(u_-^0, u_+^0)$. Then from (3.11), with $u_- = u_-^0$ we find that $v(u) > 0$ for $u_-^0 < u < u_+^0$. Consequently, comparing the unstable manifold from $(u_-^0, 0)$ to the stable manifold entering $(u_+^0, 0)$ we conclude that $\hat{R}(u_-^0, u_+^0, \tau^0) > 0$. This corresponds to the phase portrait shown in Figure 3.2a.

Let u_* be defined by (3.5) when $u_\gamma(u_*) = 1$. Next we argue that $\hat{R}(u_-^0, u_+, \tau^0) < 0$ for $u_-^0 < u_*$ and u_+ near 1. Suppose for a contradiction that $v(u) > 0$ for $u \in (u_-^0, u_+]$ and so $\hat{R}(u_-^0, u_+, \tau^0) > 0$. From (3.18),

$$\int_{u_-^0}^{u_+} G(u; u_-^0, s(u_-^0, u_+))\, du \to -\infty, \quad \text{as} \quad u_+ \to 1^-.$$

However, $\int_{u_-}^{u} v(u)\,du$ is uniformly bounded. Thus the right hand side of (3.11) is negative for u_+ close enough to 1 while the left hand side of (3.11) is positive for all u. This contradiction implies $v(u) = 0$ for some $u < u_+$, as in 3.2b.

For (u_-, u_+) on the curve A, $(u_-, 0)$ is a saddle-node equilibrium. In fact, the equilibrium has a positive eigenvalue $\lambda_+ = \beta$ and a well defined eigenvector with corresponding unstable manifold. For this reason, as in [16], the separation function $\hat{R}(u_-, u_+, \tau)$ is well defined on A and continuous on $U \cup A \cup \Sigma_\infty$, where U is the open region bounded by A, Σ_∞ and the line $u_+ = 1$.

As in the previous paragraph, since $\int_{u_-}^{u_+} G(u; u_-, s)\,du \to -\infty$ as $u_+ \to 1$, we conclude that $\hat{R} < 0$ for (u_-, u_+) on A near $(u_*, 1)$. We also observe that $\hat{R}(u_-, u_+, \tau) \to 0$ as $(u_-, u_+) \to (u_I, u_I)$. Setting $\hat{R}(u_I, u_I, \tau) = 0$, we define $\underline{u} = min\{u_- : \hat{R}(u_-, u_\gamma(u_-), \tau) = 0, u_* < u_- \le u_I\}$. Consequently, $\hat{R}(u_-, u_\gamma(u_-), \tau) < 0$ for $u_* < u_- < \underline{u}$.

For each u_-, $0 < u_- < \underline{u}$, we have identified values of u_+ at which $\hat{R}$ has opposite signs. Thus, by continuity, there exists a value of $u_+ = u_\Sigma(u_-, \tau)$ for which $\hat{R} = 0$. With existence established, we note that uniqueness follows directly from assumption (3.19).

It follows from (3.19) and the Implicit Function Theorem that u_Σ is a C^∞ function. Differentiating $\hat{R}(u_-, u_\Sigma(u_-, \tau), \tau) = 0$ with respect to τ, we find:

$$\frac{\partial \hat{R}}{\partial u_+}\frac{\partial u_\Sigma}{\partial \tau} + \frac{\partial \hat{R}}{\partial \tau} = 0. \tag{3.20}$$

But $\dfrac{\partial \hat{R}}{\partial \tau} = \dfrac{\partial R}{\partial \beta}\dfrac{\partial \beta}{\partial \tau} < 0$ from (3.8) and $\beta = 1/\sqrt{s\tau}$. It now follows from (3.19) and (3.20) that $\dfrac{\partial u_\Sigma}{\partial \tau} < 0$.

Similarly differentiating $\hat{R}(u_-, u_\Sigma, \tau) = 0$ with respect to u_-,

$$\frac{\partial \hat{R}}{\partial u_-} + \frac{\partial \hat{R}}{\partial u_+}\frac{\partial u_\Sigma}{\partial u_-} = 0. \tag{3.21}$$

But

$$\begin{aligned}\frac{\partial \hat{R}}{\partial u_-} &= \frac{\partial R}{\partial u_-} + \frac{\partial R}{\partial s}\frac{\partial s}{\partial u_-} + \frac{\partial R}{\partial \beta}\frac{\partial \beta}{\partial s}\frac{\partial s}{\partial u_-} \\ &< \int_{-\infty}^{\infty} e^{-\beta\xi}\frac{v^0}{H(u^0)}\frac{f'(u_-) - s}{u_+ - u_-}(u_+ - u)d\xi < 0,\end{aligned}$$

where we have combined (3.9), (3.10) and used (3.8) together with Lemma 3.2. Now it follows from (3.19) and (3.21) that $\dfrac{\partial u_\Sigma}{\partial u_-} < 0$. This completes the proof of Proposition 3.2. □

4. The Riemann Problem. In this section we solve the Riemann problem

$$u_t + f(u)_x = 0 \tag{4.1a}$$

$$u(x, 0) = \begin{cases} u_l & \text{if } x < 0 \\ u_r & \text{if } x > 0. \end{cases} \tag{4.1b}$$

Solutions of (4.1) are leading order approximations to solutions of (2.6) with jump initial data. The discontinuity is propagated as combinations of shock and rarefaction waves, suggesting the decomposition of solutions of general initial value problems for equation (2.6) into combinations of traveling waves approximating shocks, and smooth waves approximating rarefaction waves. The solution of (4.1) relies crucially on the description of undercompressive shocks, since these represent the boundary between admissible and inadmissible Lax shocks.

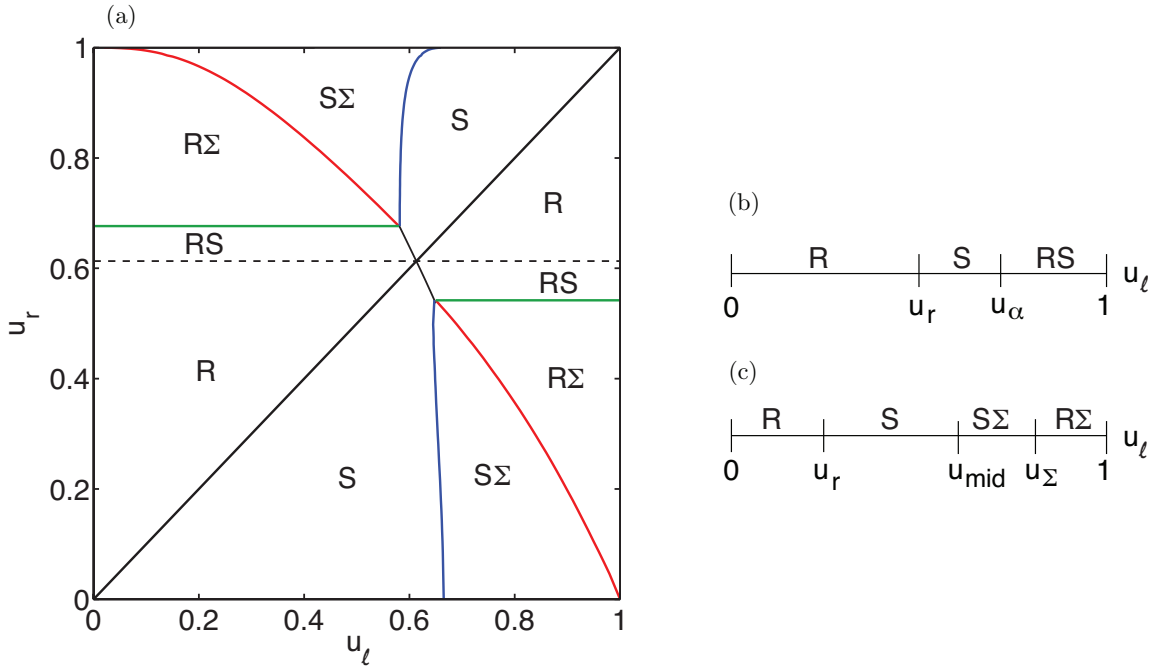

Fig. 4.1: Solution of the Riemann Problem for $\tau = 1, M = 2$: (a) solutions for all values of u_ℓ, u_r, (b) solutions as u_ℓ varies and u_r is fixed between $\bar{u}_+$ and u_I, (c) solutions as u_ℓ varies and u_r is fixed between 0 and $\underline{u}_+$. Classical solutions include rarefaction and shock waves which are denoted R and S, respectively. The notation Σ is used for the undercompressive shock solution.

In Figure 4.1, we represent the solution of the Riemann problem for all data (4.1b). The structure of the solution is independent of $\tau > 0$, so for definiteness we show the solution schematically for $\tau = 1$. In Figure 4.1a open regions are labeled according to the combination of shock and rarefaction waves appearing in the solution: classical rarefaction and shock waves are denoted by R and S, respectively, while nonclassical undercompressive shocks are denoted by Σ. The horizontal dashed line is located at $u_r = u_I$, the inflection point of $f(u)$. The horizontal lines at $u_r = \underline{u}_+$ and $u_r = \bar{u}_+$ form the boundaries between the regions labeled RS and $R\Sigma$. The curve separating regions $R\Sigma$ and $S\Sigma$ is the set of points (u_ℓ, u_r) for which there is an undercompressive shock from u_ℓ to u_r (as in Figure 3.3a). The curves separating S and $S\Sigma$ represent the middle equilibria of undercompressive shocks: they consist of pairs (u_{mid}, u_r), for which $u_{mid} = u_{mid}(u_-)$ is the middle equilibrium for some u_- and $u_r = u_\Sigma(u_-)$ is the right state of an undercompressive shock. Since these curves are monotonic, it is convenient to parameterize them by u_r. Accordingly, we let $u_o(u_r) = u_{mid}^{-1}(u_r), u_\sigma(u_r) = u_\Sigma^{-1}(u_r)$. The short curve through the point (u_I, u_I) consists of the points $(u_\alpha(u_r), u_r)$. It is part of the curve labeled 'A' in Figure 3.1b.

We describe solutions of the Riemann problem by fixing $u_r < u_I$ in two cases (the construction for $u_r > u_I$ is similar) and varying u_ℓ. This approach is simpler than fixing u_ℓ, as in [7], which involves many more cases and is more complicated because of the shape of the curves separating regions S and $S\Sigma$.

- For $\bar{u}_+ < u_r < u_I$ (Figure 4.1b), the Riemann problem has only classical solutions as u_ℓ varies between 0 and 1. When $u_\ell < u_r$, a rarefaction wave joins the two states as, in this region, characteristic speeds are increasing from u_ℓ to u_r. An admissible Lax shock from u_ℓ to u_r exists when $u_\ell \in (u_r, u_\alpha(u_r))$. For $u_\alpha(u_r) < u_\ell < 1$, the solution is a rarefaction-shock, a combination of a rarefaction wave from u_ℓ to $u_\alpha(u_r)$ and an admissible Lax shock between $u_\alpha(u_r)$ and u_r with speed

$f'(u_\alpha(u_r))$.

- For $0 < u_r < \underline{u}_+$ (Figure 4.1c), solutions are either classical or a combination of classical and nonclassical waves, depending on the value of u_ℓ. As in the previous case, a rarefaction wave joins u_ℓ to u_r when $u_\ell < u_r$. Recall that $u_o = u_o(u_r), u_\sigma = u_\sigma(u_r)$ are the middle and top equilibria for the undercompressive shock from u_σ to u_r. The graphs of these functions form the boundaries between the regions $S, S\Sigma, R\Sigma$. For $u_\ell \in (u_r, u_o)$, the solution to (4.1) is an admissible Lax shock. Once $u_\ell > u_o$, an admissible Lax shock connects u_ℓ to u_σ and then an admissible undercompressive shock joins u_σ and u_r. This structure persists as long as $u_\ell < u_\sigma$. Finally, for $u_\sigma < u_\ell < 1$, the solution is a combination of a rarefaction wave from u_ℓ to u_σ and an admissible undercompressive shock from u_σ to u_r.

It is worth pointing out that by construction, even though double shock solutions $S\Sigma$ of the Riemann problem are not monotonic, nonetheless the values of u remain in the physically valid interval $0 \le u \le 1$. As we have seen in the construction of traveling waves for undercompressive shocks, this is a consequence of the degeneracy of $H(u)$ at $u = 0, 1$.

As $\tau \to 0$, we have $\beta = 1/\sqrt{s\tau} \to \infty$ since $1 \le s \le f'(u_I)$. To understand this limit, let $\xi = \beta\zeta$ so that (2.12) becomes

$$\frac{1}{\beta^2}u'' = u' + \frac{1}{H(u)}\left[s(u-u_-) - f(u) + f(u_-)\right],$$

in which $' = d/d\zeta$. In the limit $\beta \to \infty$, this ODE reduces to

$$u' = -\frac{1}{H(u)}\left[s(u-u_-) - f(u) + f(u_-)\right].$$

Consequently, the traveling waves connect only adjacent equilibria u_-, u_+ satisfying the Rankine-Hugoniot condition (2.11), corresponding to Lax shocks. The solution of the Riemann problem (4.1) is therefore entirely classical. This is manifested in Figure 4.1a by the curves Σ_τ (separating regions $R\Sigma$ and $S\Sigma$ in the figure) approaching the horizontal lines $u_+ = 0$ and $u_+ = 1$, thereby collapsing the regions indicating undercompressive shocks.

5. PDE Simulations. To verify the solution structures obtained in the previous section, we numerically simulate solutions of (2.7) with jump initial data (4.1b) and $\tau = 1, M = 2$. Computations are performed on the interval $-2 \le x \le 4$, with $\Delta x = h = 0.002$ for the rarefaction and rarefaction-undercompressive shock solutions and $h = 0.005$ in other cases. All solutions are shown at time $t = 1$, with $\Delta t = k = 0.1\,(\Delta x)^2$. The pairs (u_ℓ, u_r) are chosen in each case by consulting Fig. 4.1a; for example, we choose $(u_\ell, u_r) = (0.8, 0.2)$ to generate the shock-undercompressive shock solution so that the size of the jumps and separation between shocks are clear in the plots.

By scaling x and t by a small parameter ϵ, we can control the effects of the regularization terms in (2.7). In particular, traveling waves then have width on the order of ϵ. With this scaling, (2.7) becomes

$$\frac{\partial u}{\partial t} + \frac{\partial f(u)}{\partial x} = \frac{\partial}{\partial x}\left[H(u)\left(\epsilon\frac{\partial u}{\partial x} + \epsilon^2\tau\frac{\partial^2 u}{\partial x \partial t}\right)\right].$$

The corresponding finite difference scheme is:

$$\begin{aligned}
&\frac{u_j^n - u_j^{n-1}}{k} + \frac{g_{j+1/2} - g_{j-1/2}}{h} = \\
&\frac{\epsilon}{h^2}\left[H\left(\bar{u}^n_{j+\frac{1}{2}}\right)(u^n_{j+1} - u^n_j) - H\left(\bar{u}^n_{j-\frac{1}{2}}\right)(u^n_j - u^n_{j-1})\right] + \\
&+\frac{\epsilon^2\tau}{h^2 k}\left[H\left(\bar{u}^n_{j+\frac{1}{2}}\right)(u^n_{j+1} - u^n_j - u^{n-1}_{j+1} + u^{n-1}_j) - H\left(\bar{u}^n_{j-\frac{1}{2}}\right)(u^n_j - u^n_{j-1} - u^{n-1}_j + u^{n-1}_{j-1})\right].
\end{aligned} \tag{5.1}$$

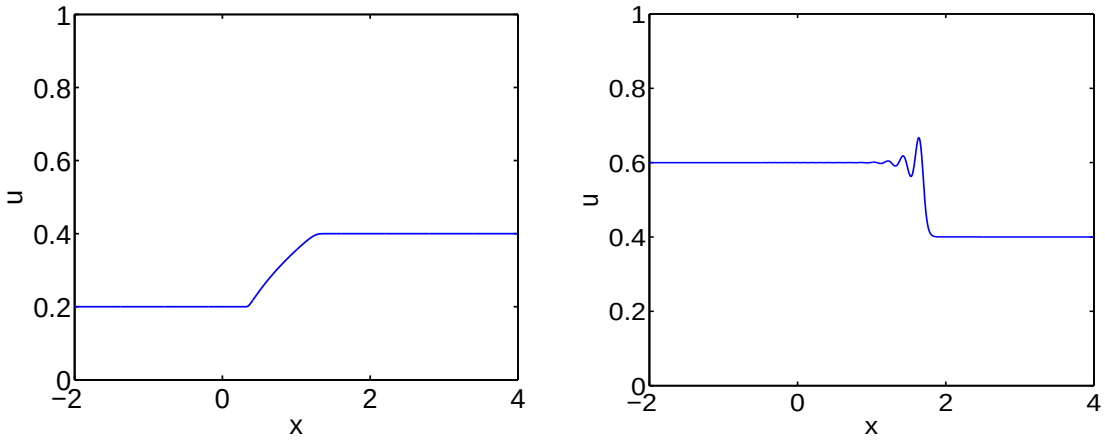

(a) (b)

Fig. 5.1: (a) Rarefaction wave solution for $u_\ell = 0.2, u_r = 0.4, \epsilon = .01, \tau = 1, M = 2$. (b) Admissible Lax shock for $u_\ell = .6, u_r = .6, \epsilon = .05, \tau = 1, M = 2$.

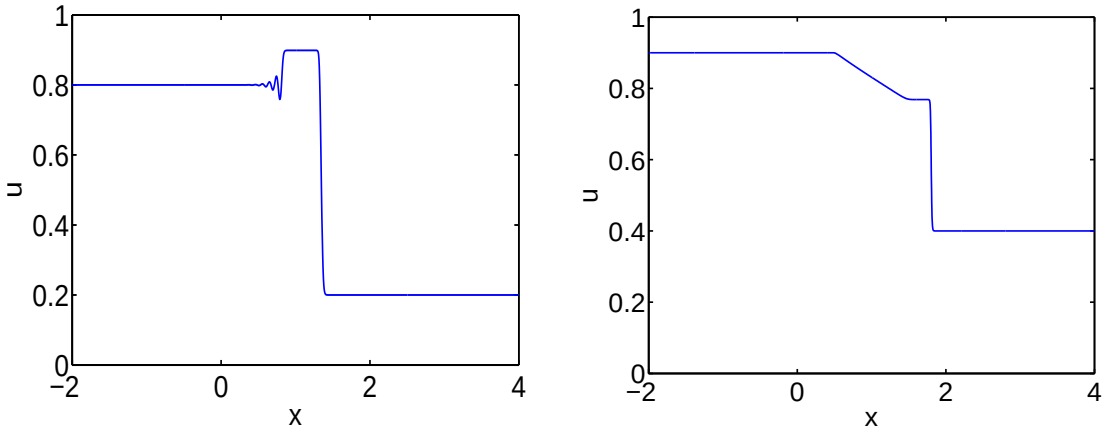

(a) (b)

Fig. 5.2: (a) Admissible Lax shock trailing the undercompressive shock for $u_\ell = .8, u_r = .2, \epsilon = .05, \tau = 1, M = 2$. (b) Rarefaction wave trailing the undercompressive shock for $u_\ell = .9, u_r = .4, \epsilon = .01, \tau = 1, M = 2$.

where $\bar{u}_{j+\frac{1}{2}} = \frac{1}{2}(u_j + u_{j+1})$, and $g_{j+1/2} = \frac{1}{12}(-f(u_{j+2}) + 7f(u_{j+1}) + 7f(u_j) - f(u_{j-1}))$ is a high order approximation of the flux function $f(u)$ [7]. Specifically, it has truncation error that is $O(h^3)$ and so is higher order than the truncation error from the right hand side of (5.1), which is $O(\epsilon h^2)$, provided $h \ll \epsilon$. Even though $H(u)$ is nonlinear, the modified equation has the same form as in [7]:

$$u_t + f(u)_x = \epsilon(H(u)u_x)_x + \epsilon^2\tau(H(u)u_{xt})_x + O(h^3) + O(\epsilon h^2).$$

The initial condition (4.1b) is smoothed slightly to avoid spurious small oscillations:

$$u_j(0) = -\tanh(\delta x_j)\frac{u_\ell - u_r}{2} + \frac{u_\ell + u_r}{2},$$

with $\delta = 250$ in these simulations.

In Figure 5.1a, a smooth rarefaction wave connects $u_\ell = 0.2$ to $u_r = 0.4$. The classical Lax shock from $u_\ell = 0.6$ to $u_r = 0.4$ is shown in Figure 5.1b. In Figure 5.2a, there is a Lax shock from $u_\ell = 0.8$ to the plateau value of u_σ, and a faster undercompressive shock from u_σ to $u_r = 0.2$. Both shock solutions have exponentially decaying oscillations behind the Lax shock due to the complex eigenvalues at u_ℓ. The oscillation wavelengths can be computed from the coefficients of the eigenvalues' imaginary parts (see (3.1); accounting also for ϵ), and compare well with the distances between successive maxima in the plots. For these two simulations, $\epsilon = 0.05$ in order to show the oscillations clearly. When the simulations are done with $\epsilon = 0.01$ the predicted oscillations are too compressed to be seen clearly. Finally, Figure 5.2b illustrates the rarefaction-undercompressive shock solution. The rarefaction wave connects $u_\ell = 0.9$ to u_σ and the undercompressive shock takes u_σ to $u_r = 0.4$.

6. Concluding Remarks. With the inclusion of dynamic capillary pressure, the Buckley-Leverett equation admits traveling waves corresponding to undercompressive shocks. For relative permeabilities that depend quadratically on saturation, we have completely characterized undercompressive shocks and solutions of the Riemann problem. It would be interesting to use these solutions to investigate the Cauchy problem using wave front tracking, modifying the analysis in [13]. For numerical purposes, we have chosen specific values of the parameters; due to the robust nature of the analysis, the broad structure of our results can be expected to hold for more general relative permeability functions.

Propagating fronts in secondary oil recovery are known to be typically subject to viscous fingering [9]. On the other hand, undercompressive shocks in other contexts have been shown to be stable to transverse perturbations [1]. It would be interesting to know whether the traveling waves in this paper are stable to two-dimensional perturbations, since these undercompressive waves represent the leading edge of the oil-water transition in secondary oil recovery.

Acknowledgement. The authors thank Steve Schecter for valuable discussions of the separation function.

REFERENCES

[1] A. L. Bertozzi, A. Münch, M. Shearer, and K. Zumbrun. Stability of compressive and undercompressive thin film travelling waves. *Euro. J. of Appl. Math.*, 12(03):253–291, 2001.
[2] S. E. Buckley and M. C. Leverett. Mechanism of fluid displacement in sands. *Petroleum Trans. AIME*, 146:107–116, 1942.
[3] C. Cuesta, C. J. van Duijn, and J. Hulshof. Infiltration in porous media with dynamic capillary pressure: travelling waves. *Euro. J. of Appl. Math.*, 11:381–397, 2000.
[4] C. M. Cuesta, C. J. van Duijn, and I. S. Pop. Non-classical shocks for Buckley-Levertt: Degenerate pseudo-parabolic regularisation. In A. Di Bucchianico, R. M. M. Mattheij, and M. A. Peletier, editors, *Progress in Industrial Mathematics at ECMI 2004*, Mathematics in Industry 8, pages 569–573. European Consortium for Mathematics in Industry, Springer Berlin Heidelberg, 2006.
[5] S. M. Hassanizadeh and W. G. Gray. Mechanics and thermodynamics of multiphase flow in porous media including interphase boundaries. *Adv. Water Resour.*, 13:169–186, 1990.
[6] S. M. Hassanizadeh and W. G. Gray. Thermodynamic basis of capillary pressure in porous media. *Water Resour. Res.*, 29:3389–3405, 1993.
[7] B. Hayes and M. Shearer. Undercompressive shocks and Riemann problems for scalar conservation laws with non-convex fluxes. *Proc. Roy. Soc. Edinburgh Sect. A*, 129:733–754, 1999.
[8] R. Helmig, A. Weiss, and B. J. Wohlmuth. Dynamic capillary effects in heterogeneous porous media. *Comp. Geosciences*, 11:261–274, 2007.
[9] G. M. Homsy. Viscous fingering in porous media. *Ann. Rev. Fluid Mech.*, 19(1):271–311, 1987.
[10] J. Hulshof and J. R. King. Analysis of a Darcy flow model with a dynamic pressure saturation relation. *SIAM J. Appl. Math.*, 59:318–346, 1998.

[11] D. Jacobs, W. R. McKinney, and M. Shearer. Traveling wave solutions of the modified Korteweg-de Vries-Burgers equation. *J. Differential Eqns.*, 116:448–467, 1995.
[12] P. D. Lax. Hyperbolic systems of conservation laws ii. *Comm. Pure Appl. Math.*, 10:537–566, 1957.
[13] P. G. LeFloch. *Hyberbolic Systems of Conservation Laws. The Theory of Classical and Nonclassical Shock Waves*. Lectures in Math. Birkhauser Verlag, Zurich, 2002.
[14] Sabine Manthey, S. Majid Hassanizadeh, Rainer Helmig, and Rudolf Hilfer. Dimensional analysis of two-phase flow including a rate-dependent capillary pressure-saturation relationship. *Adv. Water Resources*, 31(9):1137–1150, 2008.
[15] D. Peaceman. *Fundamentals of Numerical Reservoir Simulation*. Elsevier Scientific Pub. Co., Amsterdam; New York, 1977.
[16] S. Schecter. The saddle-node separatrix-loop bifurcation. *SIAM J. Math. Anal.*, 18(4):1142–1156, 1987.
[17] A. E. Scheidegger. *The Physics of Flow Through Porous Media*. University of Toronto Press, New York, 1960.
[18] J. A. Trangenstein. *Numerical Solution of Hyperbolic Partial Differential Equations*. Cambridge University Press, Cambridge, 2007.
[19] C. J. van Duijn, L. A. Peletier, and I. S. Pop. A new class of entropy solutions of the Buckley-Leverett equation. *SIAM J. Math. Anal.*, 39(2):507–536, 2007.